Smart Materials and Structures

PURPOSE-LED PUBLISHING™

LETTER • **OPEN ACCESS**

Compression and fatigue performance of additively manufactured NiTi architected shape memory alloys

To cite this article: Borit Zwerink *et al* 2025 *Smart Mater. Struct.* **34** 09LT02

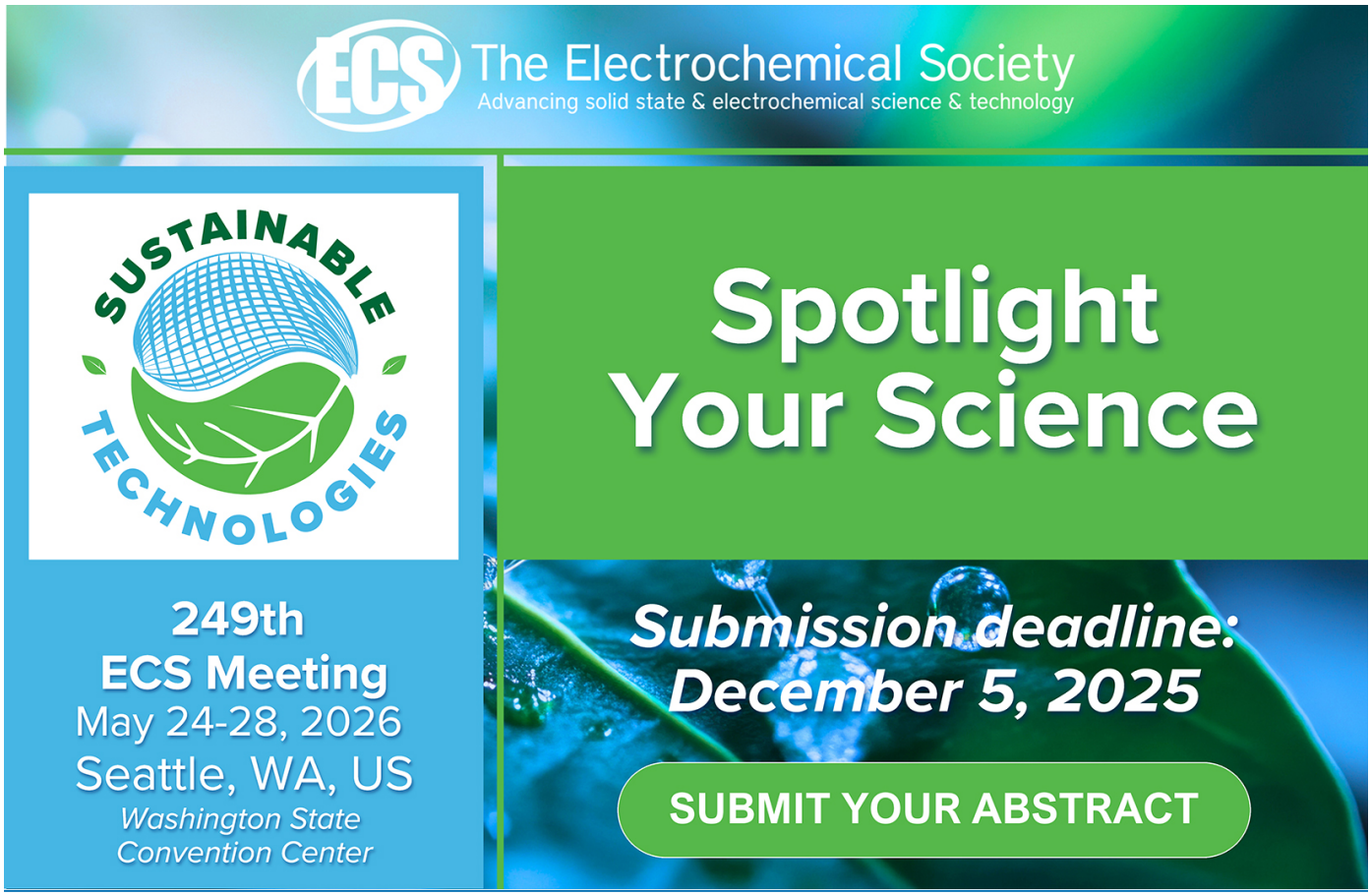

OPEN ACCESS
IOP Publishing

Letters
Smart Materials and Structures

Smart Mater. Struct. **34** (2025) 09LT02 (10pp)
https://doi.org/10.1088/1361-665X/ae0904

Letter

Compression and fatigue performance of additively manufactured NiTi architected shape memory alloys

Borit Zwerink[1], Carlo Alberto Biffi[2], Jacopo Fiocchi[2] and Mehrshad Mehrpouya[3,*]

[1] NLR Royal Netherlands Aerospace Centre, Marknesse, The Netherlands
[2] National Research Council, CNR-ICMATE, Lecco, Italy
[3] Faculty of Engineering Technology, University of Twente, Enschede, 7500, AE, The Netherlands

E-mail: m.mehrpouya@utwente.nl

Received 14 June 2025, revised 7 September 2025
Accepted for publication 18 September 2025
Published 25 September 2025

Abstract

Additive manufacturing of architected materials—particularly lattice or porous structures—has gained significant attention in recent years due to their enhanced strength-to-weight ratios, load-bearing capabilities, and energy absorption properties. The integration of these structures with shape memory alloys offers multifunctional performance for advanced engineering applications. This study investigates the compressive fatigue behavior of NiTi lattice structures fabricated by Laser powder bed fusion. Initial quasi-static compression tests, carried out to full structural collapse, were used to define load levels for subsequent fatigue experiments. Fatigue testing was then conducted at 40 °C to induce pseudoelastic behavior, and an S–N curve was generated to characterize fatigue performance. Results showed that the NiTi lattice could sustain cyclic loading at 8 kN for an average of approximately 86 000 cycles, and around 18 000 cycles at 11 kN. Post-mortem microstructural analyses revealed martensite accumulation near fracture regions, attributed to stress-induced phase transformation.

Keywords: additive manufacturing, LPBF, shape memory alloys, NiTi, architected structures, fatigue

1. Introduction

In recent years, considerable efforts have been directed toward enhancing structural functionality through the integration of the inherent capabilities of shape memory alloys (SMAs) [1, 2]. The remarkable flexibility and freeform capacity of additive manufacturing (AM) technologies have shown significant promise in fabricating SMAs, thus opening up new avenues of opportunity by enabling the creation of intricate geometries, like complex shape lattice structures, previously unattainable with conventional manufacturing techniques [3, 4]. One of the most encouraging potential applications of AM SMAs is in the fabrication of lattice or porous structures with shape recovery performance, so that they can retrieve their original shape [5–7]. These structures have demonstrated remarkable thermomechanical performance in terms of light-weight properties [8–10], improved damping abilities [11], high energy absorption [12, 13], and high specific strength and stiffness [14–17].

Architected NiTi structures produced by AM are typically designed for conditions in which compressive forces predominate. One of the advantages of AM technology in

* Author to whom any correspondence should be addressed.

fabricating these types of structures is the ability to optimize parameters such as strut diameter, strut length, wall thickness, or unit cell configuration [18–23]. This optimization is particularly beneficial for tuning the mechanical performance of such lattices as well as load bearing, Young's modulus of components, and energy absorption applications [24–28]. For example, there is a report on improvement in the design of NiTi-SMA gradient lattice structure by outstanding shape memory effect and functional stability with a larger displacement recovery interval of up to 99% for the unidirectional setup and an accumulative irrecoverable strain up to 0.8% which showed the excellent compression energy absorption [29]. In another study, enhancement in the architected design of Fe-based SMA through AM techniques demonstrated increased compressive strength. This improvement led to enhanced multifunctional behavior, energy absorption capacity, load-bearing ability, and geometric recoverability of the components [30].

Multiple studies have highlighted the complex fatigue behavior of superelastic Nitinol, emphasizing the influence of microstructure, loading conditions, and processing history [31–37]. For instance, Mahtabi *et al* reviewed the state-of-the-art and ongoing challenges, noting that fatigue in nitinol is more complex than in traditional alloys due to its unique superelastic and shape memory properties, with microstructural effects and testing conditions playing significant roles in fatigue life [38]. Malito *et al* established a methodology for determining small crack growth thresholds, finding that small cracks—comparable to native inclusions—are critical for predicting fatigue lifetime in medical devices [39]. Launey *et al* demonstrated that pre-strain, mean strain, temperature, and strain amplitude all significantly affect the fatigue response, and they proposed both empirical and energy-based models for predicting fatigue strain limits [40]. Pelton *et al* found that pre-strain and mean strain can either enhance or degrade fatigue performance, with cycling in the two-phase region generally leading to longer fatigue lives due to martensite stabilization and cyclic phase transformation [41]. Gugat *et al* reported excellent high-cycle fatigue resistance in sputtered nitinol thin films, with a fatigue safety limit of 1.75% strain amplitude for mean strains up to 2.5% [42]. Additionally, Shabani Nezhad *et al* showed that wire size and microstructural inhomogeneities introduced during processing significantly influence fatigue behavior, with smaller wires being more vulnerable to surface defects but exhibiting better functional performance [43]. These findings collectively underscore the importance of microstructural control, loading history, and device geometry in optimizing the fatigue performance of superelastic nitinol.

Alarcon *et al* reported a significant reduction in the fatigue performance of NiTi wires, particularly when loading approaches the stress-induced martensitic transformation (MT) regime, which results in large recoverable strains due to the superelastic effect [44]. Similarly, Sherif *et al* demonstrated successful fatigue cycling of NiTi wires and explored the influence of various parameters, such as maximum tensile stress and residual strain, on the material's cyclic performance. However, the fatigue behavior of NiTi SMA lattice structures under varying stress conditions presents a distinct research direction. These investigations highlight the potential of tailored design strategies to achieve high-cycle functional performance, which is particularly critical for biomedical applications like stents [45]. It is important to note that the functional longevity of a printed component is not determined solely by structural failure; high functional fatigue life is equally important and can be heavily influenced by lattice geometry.

Despite this, most existing studies have focused on the limited cycling behavior of SMA lattices, underscoring the need for further research involving extended fatigue cycles [46–49]. The interplay between geometric design and scanning strategy plays a vital role in fatigue performance, as it governs the initiation and growth of defects or inclusions that can severely degrade the material's endurance [50]. For instance, Chen *et al* demonstrated that careful component design can lead to enhanced fatigue life in NiTi lattice structures [29]. Biffi *et al* investigated the cyclic compression and shape recovery of NiTi architected meta-structures produced via the laser powder bed fusion (LPBF) process, employing three different compression loads to assess a broad range of shape recovery behavior and energy dissipation characteristics [51, 52]. Similarly, Speirs *et al* reported that the fatigue performance of NiTi structures is strongly influenced by design features that generate stress concentrations and facilitate crack initiation [53], a finding further validated by Ren *et al* in a separate study [54].

This study examines fatigue behavior over an extended range of cycles. Fatigue tests are conducted under varying load levels to enable the development of an S–N curve tailored specifically to the NiTi lattice structure. Additionally, the relationship between transformation temperatures and the evolving microstructure in different regions of the tested samples is analyzed to provide insights into how the material's properties change throughout cyclic loading. This approach enhances the understanding of the material's behavior and phase transformations during the experimental process.

2. Experimental procedure

Spherical Ni-rich NiTi powder (Ni56Ti44 wt.%) with a particle size of 16–63 μm (Nanoval, Germany) was processed using an LPBF system (Renishaw AM400, UK). The process parameters were optimized to achieve a 99.5% relative density of [51]. Table 1 reports the adopted process parameters.

The architected structures investigated in this study exhibit auxetic behavior, characterized by a negative Poisson's ratio, as reported in our previous work [51, 52] and illustrated in figure 1. A total of ten NiTi samples were fabricated in a horizontal orientation on the build platform and subsequently heat-treated at 500 °C for 5 min, followed by water quenching. Samples 1 and 2 were subjected to monotonic compression tests to determine the maximum compressive force leading to failure, while Samples 3 through 10 were allocated for fatigue testing.

Compression tests were performed at room temperature with a 100 kN load cell, using a crosshead speed of

Table 1. List of process parameters used for the printing of the architected NiTi samples.

Laser power	Exposure time	Oxygen level	Atmosphere	Layer thickness	Hatch distance	Laser spot size	Point distance	Scanning strategy
150 W	75 μs	<20 ppm	Argon	30 μm	50 μm	65 μm	120 μm	Meander

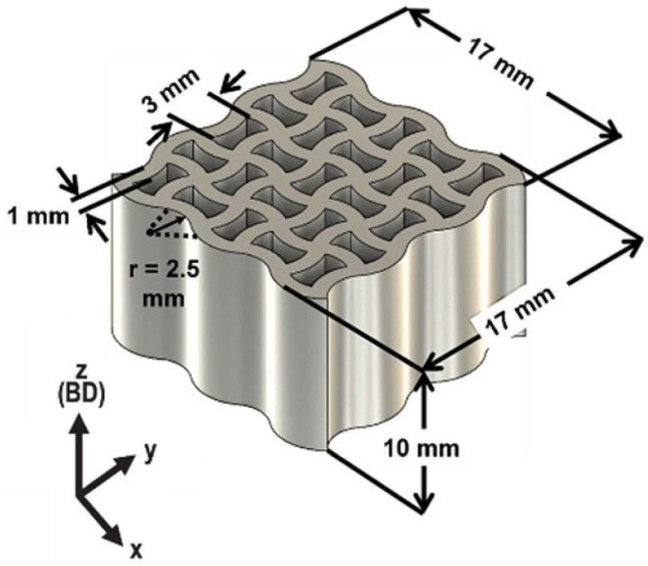

Figure 1. CAD model, highlighting the principal dimensions of the investigated architected structure [55]. Reproduced from [55]. CC BY 4.0.

1 mm min^{-1} (Instron 5989). Once the failure force was identified, fatigue tests were conducted at 5 Hz with a stress ratio of R = 0.1, varying the applied load at three levels (MTS 810). Before testing, samples were heated to 40 °C to maintain the austenite phase. Specifically, three samples (5–7) were tested at a maximum load of 8 kN, two (3–4) at 9 kN, and three (8–10) at 11 kN. Given the stress ratio of 0.1, the corresponding minimum loads were 0.8, 0.9, and 1.1 kN, respectively. Based on the effective cross-sectional area of the samples (60 mm2), this corresponds to maximum stress amplitudes of approximately 133, 150, and 183 MPa. The lattice specimen has a nominal (projected) cross-sectional area of 10 mm × 15 mm (150 mm^2). However, due to its geometry, the structure consists of 6 individual struts, each approximately 1 mm wide and spanning the full 10 mm depth. Therefore, the effective cross-sectional area is estimated to be 6 × 1 mm × 10 mm (60 mm^2).

After the fatigue testing, the fractured regions of the samples were observed with Optical Microscopy (Keyence, Model VHX-1000) at low magnification and scanning electron microscopy (Nova, Model NanoSEM450) at high magnification. Furthermore, the results obtained from electron backscattered diffraction (EDAX Trident system) were correlated to study the microstructural evolution of the tested samples. The MT temperatures were measured using differential scanning calorimetry (DSC, Q25 model, TA Instruments, USA). The analysis was conducted with a heating/cooling rate of 10 °C min^{-1} over a temperature range of −50 °C to 100 °C. DSC was performed on the as-built samples and two samples after fatigue analysis.

3. Results and discussion

The mechanical behavior of the architected structures was evaluated through compression tests on two samples (Samples 1 and 2) until fracture. The corresponding force-displacement curves (figure 2(a)) show an initial linear increase in load up to approximately 0.35 mm of displacement, followed by a second slope leading to structural collapse at around 20 kN. This second, shallower slope likely reflects a transition from purely elastic deformation to localized structural rearrangement or the onset of plastic deformation within the architecture, such as buckling of struts or progressive failure at critical nodes. This behavior stabilizes until reaching a maximum displacement between 1.0 and 1.25 mm. Notably, this transition occurs at approximately 10 kN, indicating that this load range may be of interest for further study.

Fatigue tests in compression were conducted at 40 °C to assess the functional performance of NiTi architected structures under high-cycle conditions. At this temperature, the material is fully austenitic, as the austenite finish temperatures (A_f) of all samples, determined via DSC, are well below 40 °C (see figure 5). While fatigue testing occurred in the austenitic state, it is possible that MT occurred during post-test SEM analysis at room temperature. Loads of 8, 9, and 11 kN were applied to determine the S–N curves, with figures 2(b)–(d) illustrating the deformation evolution per cycle under different load conditions. Higher loads resulted in greater deformation and a shorter lifespan, highlighting the load-dependent nature of the fatigue response. Notably, among the samples tested at 11 kN (Samples 8, 9, and 10), Sample 9 failed significantly earlier than the others, 13 841 cycles vs. 19 898 and 20 960 cycles for Samples 8 and 10, respectively. This discrepancy may be attributed to variations in the LPBF process affecting the internal structure, such as porosity or local residual stresses. Additionally, the initial deformation at the start of each test was approximately 0.2 mm, except for the 11 kN tests, where it was noticeably higher.

Figures 3(a)–(c) presents the stress–position hysteresis loops for three additively manufactured NiTi lattice samples (Samples 4, 6, and 10), tested under cyclic compressive fatigue loading at maximum force levels of 9 kN, 8 kN, and 11 kN, respectively. Selected cycles are shown to illustrate the evolution of mechanical behavior throughout fatigue life. The hysteresis loops are plotted using stress versus crosshead displacement, rather than true strain, as direct strain measurements were not available. In this study, strain was approximated from global displacement. Whereas this approach introduces some limitations due to machine compliance and boundary effects, the stress–displacement curves still provide meaningful and consistent insights into energy dissipation and deformation trends across samples.

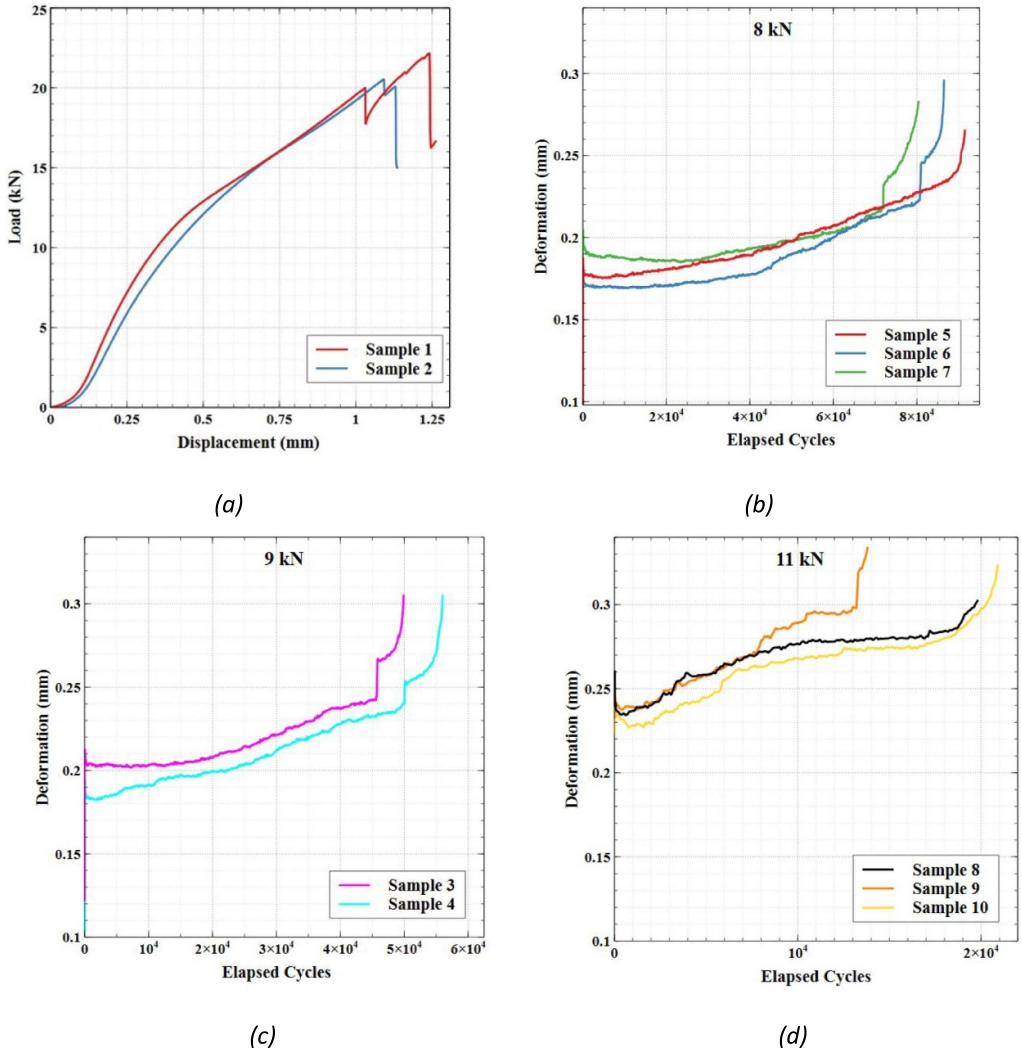

Figure 2. (a) Compression test results for Samples 1 and 2; (b)–(d) deformation per cycle until failure for samples tested under different loads.

In all cases, the applied force range was held constant during testing. Since the cross-sectional area of the samples remained unchanged, the peak compressive stress values remained stable over the fatigue life. This indicates that the samples maintained their load-bearing capacity and exhibited a stable superelastic response during the initial and intermediate stages of cycling.

Despite the differences in load levels, all samples demonstrated similar cyclic behavior. A gradual accumulation of residual deformation was observed over the course of the tests, accompanied by a progressive reduction in the slopes of both the loading and unloading curves—indicative of stiffness degradation. These effects became more pronounced in the final cycles before failure, where the hysteresis loops widened and the slopes decreased significantly, reflecting increased energy dissipation and a marked loss of structural integrity. Among the three, Sample 10 (tested at the highest load of 11 kN) consistently showed greater deformation throughout the test, consistent with the higher strain response expected under elevated loading conditions.

The energy dissipated per cycle was estimated by calculating the area enclosed by the stress–position hysteresis loop, with strain approximated by dividing the crosshead displacement by the specimen's initial height. Figure 3(d) shows the evolution of energy dissipation over the fatigue life for each sample. As expected, the sample tested at the highest load (11 kN) exhibited significantly greater energy dissipation, reflecting increased internal deformation and energy loss mechanisms. In contrast, samples subjected to lower loads (8–9 kN) displayed lower and more stable dissipation trends, consistent with fatigue behavior dominated by elastic deformation. Some scatter and early increases in dissipation, particularly in Sample 9, may be attributed to microstructural settling or the onset of early damage accumulation. Overall, the consistency across samples supports the validity of the measurement approach for comparative analysis.

Figure 4(a) shows the average number of cycles to failure and the corresponding average displacement at failure for each load. The data indicates that as the maximum applied load decreases, the average number of cycles to failure increases

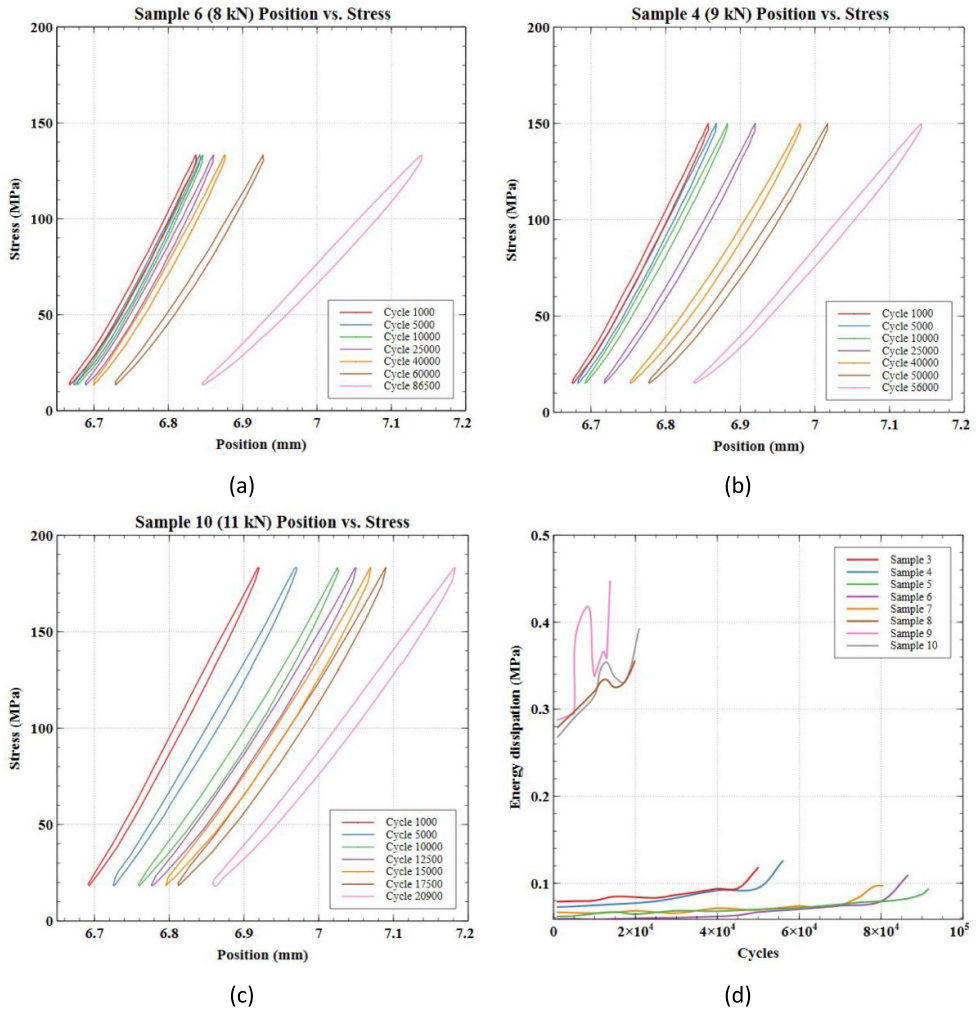

Figure 3. Stress—position hysteresis loops for the NiTi samples under different loading conditions: (a) 8 kN; (b) 9 kN; (c) 11 kN; and (d) energy dissipation over fatigue cycles for each sample.

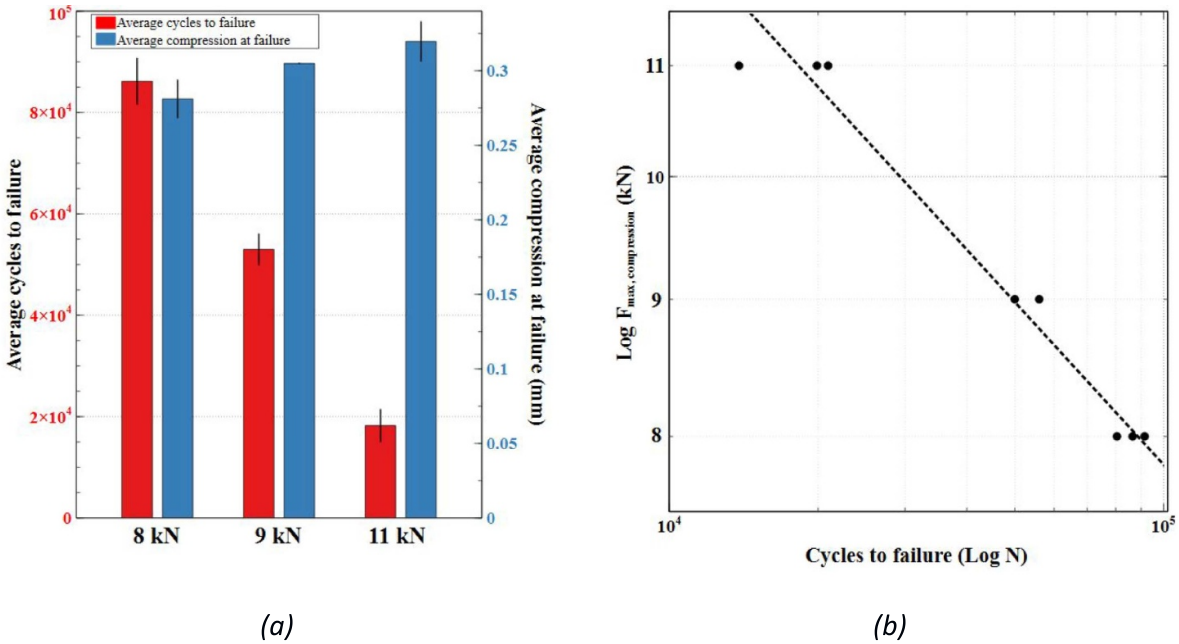

Figure 4. (a) Average cycles to failure and average compression at failure for each load; (b) S–N curve for fatigue tests on lattice samples under 8, 9, and 11 kN loads.

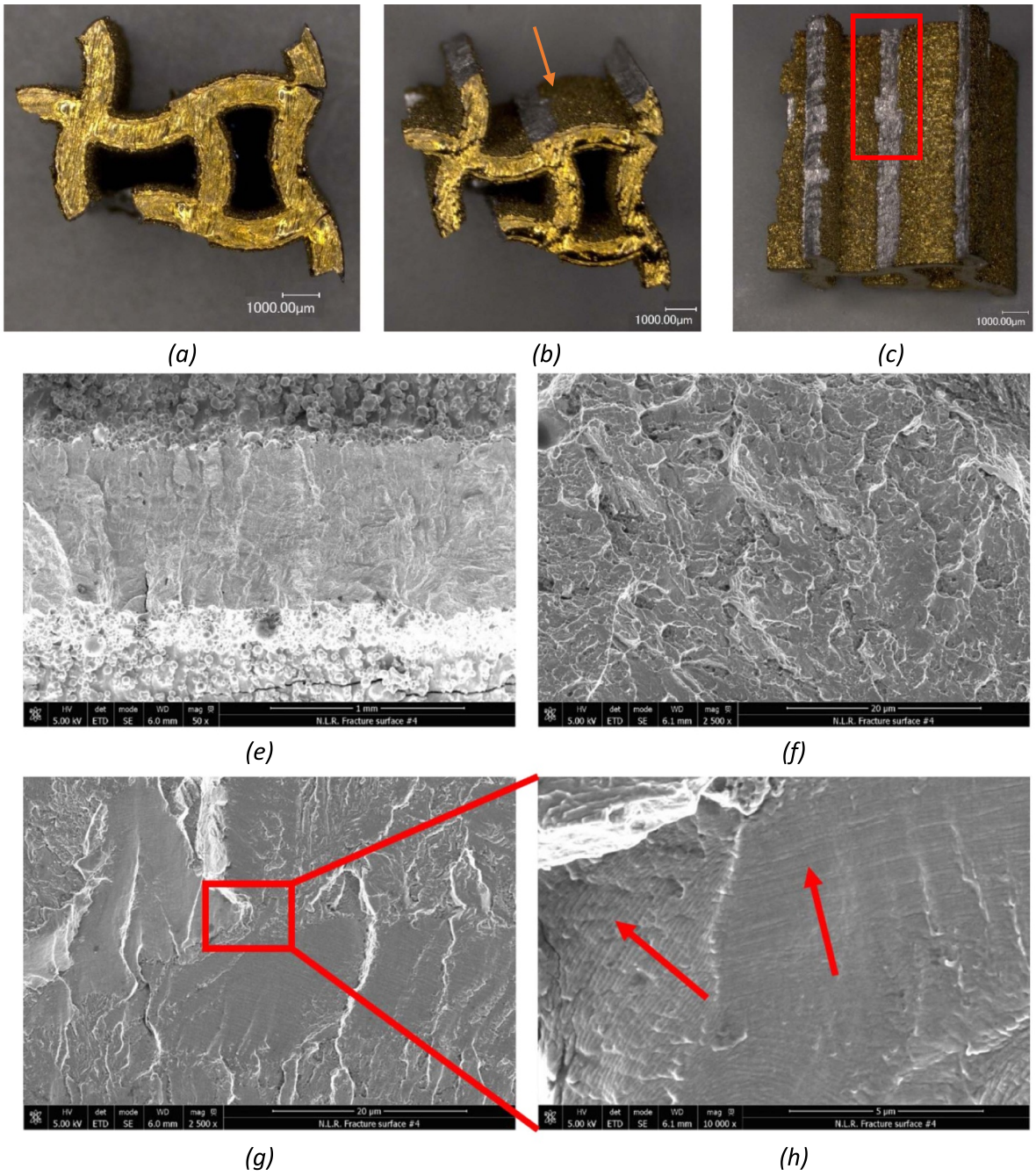

Figure 5. OM and SE-SEM images of the NiTi architected sample (Sample 4): (a) top view, (b) isometric view with an arrow indicating the fractured region for further investigation, and (c) lateral view highlighting the fractured area, with a red box marking the region for high-magnification observation. SE-SEM images of the fracture surface at increasing magnifications: (e) overview of the fractured region, (f) close-up of selected areas showing dimples and smooth subsurfaces, and (g) magnified view of the red box in (h), highlighting the striations.

from 18 000 to 86 000, while the average displacement at failure slightly decreases from 0.32 mm to 0.28 mm. The figure also illustrates the deformation progression per cycle until failure, with each graph corresponding to a specific applied load. Deformation gradually increases with each cycle, followed by a sudden spike, indicating structural failure.

Figure 4(b) presents the fatigue test results in an S–N curve, where the *y*-axis represents the logarithm of the maximum compressive force, and the *x*-axis represents the logarithm of cycles to failure. The data exhibits a strong correlation, fitting well to a power-law trend on a log–log scale.

Since the MT in NiTi SMAs can be triggered by stress, the evolution of the microstructure near the selected fracture area was examined to better understand the damage mechanisms in LPBF-fabricated NiTi lattice structures.

Figures 5(a)–(c) display OM images of a lattice sample at the end of the fatigue test. These images show a portion of the fractured sample, where a ligament detached due to exceeding

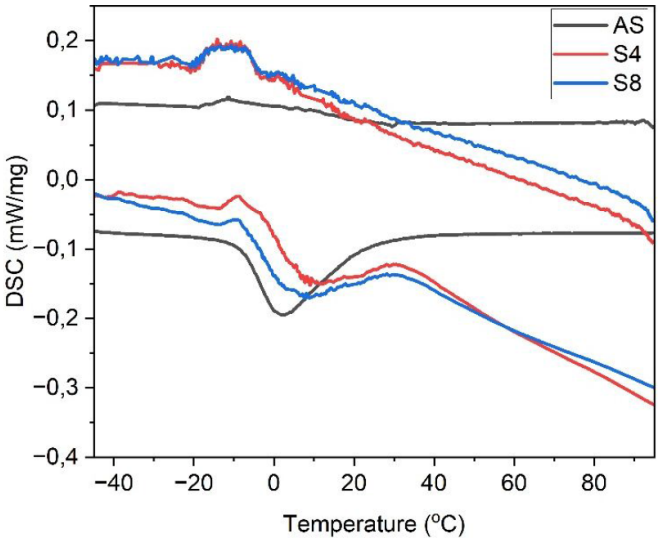

Figure 6. DSC scans of NiTi architected structures in three conditions: as-built (A_S) sample before fatigue testing, and fractured regions after testing for Samples 4 and 8.

the material's maximum load. A high-magnification SEM analysis was performed on the fracture region highlighted by the red box in figure 5(c), using the secondary electron (SE) signal.

Figure 5(e) presents an overview of the fracture surface from figure 5(c), showing remnants of unmelted powder on the outer surface. The fracture surface exhibits two main regions: an irregular surface and a smooth one, both typical of AM parts subjected to fatigue. The irregular surface (figure 5(f)) contains dimples and is associated with the early failure of adjacent material, leading to an overloaded area. In contrast, the smoother surface (figure 5(g)) displays ductile failure behavior. Continuous load cycling led to the formation of fatigue striations, visible in the high magnification shown in figure 5(h). These striations follow inclined directions, as indicated by the red arrows in figure 5(h).

Figure 6 presents the DSC results for the fractured regions of the NiTi lattice samples, specifically Samples 4 and 8, along with the as-built (A_S) sample, which was tested before fatigue. These samples were chosen for comparison due to their different load conditions and fatigue responses: Sample 4 underwent a lower load with a higher number of cycles to failure, while Sample 8 was subjected to a higher load, leading to fewer cycles to failure.

The evolution of the transformation temperatures for the three samples is summarized in table 2. The austenite finish temperature (A_f) for both fractured samples was found to be higher than that of the base material, while the other transformation temperatures were not significantly influenced by the sample condition. In contrast, the applied load during cyclic compression testing did not cause any notable changes in the transformation temperatures.

The transformation temperatures of NiTi alloys can shift due to microstructural changes such as dislocation accumulation and phase transformation fatigue. The thermal hysteresis, defined as the difference between the austenite finish (A_f) and martensite finish (M_f) temperatures,

Table 2. Transformation temperatures of the investigated samples.

	M_f	M_s	A_s	A_f
Heat-treated sample	−18.2	—	−8.8	23.9
Sample 4	−19.3	−4.2	−3.6	32.5
Sample 8	−20.2	−3.8	−6.1	30.5

increased after fatigue testing, primarily due to crack formation within the samples. This observation is supported by EBSD results (figure 7), which show that regions where cracks propagated, ultimately leading to failure of the lattice structure, also exhibited alterations in the MT. In particular, high-stress concentrations in these areas led to significant plastic deformation and the formation of stress-induced martensite.

Figure 7(a) presents an SEM image of the region of interest in Sample 4. In the central zone (figure 7(b)), no cracks were observed, and EBSD analysis confirmed that austenite was the dominant phase at room temperature. In contrast, figure 5(d) shows a magnified view of a crack propagating from the outer to the inner part of the NiTi lattice. This region exhibits a clear microstructural transition from austenite to martensite, attributed to localized stress intensification. The dark contrast in this region, typically indicative of martensite, further supports this interpretation, in agreement with previous studies [17].

Thus, elevated stress levels not only triggered microstructural changes but also facilitated crack initiation and propagation, contributing to structural degradation. Although the applied loading was uniaxial and compressive, local tensile stresses can develop due to geometric features or residual stresses, enabling crack formation. This is especially relevant in auxetic lattices, where nonuniform deformation patterns can amplify localized stress states.

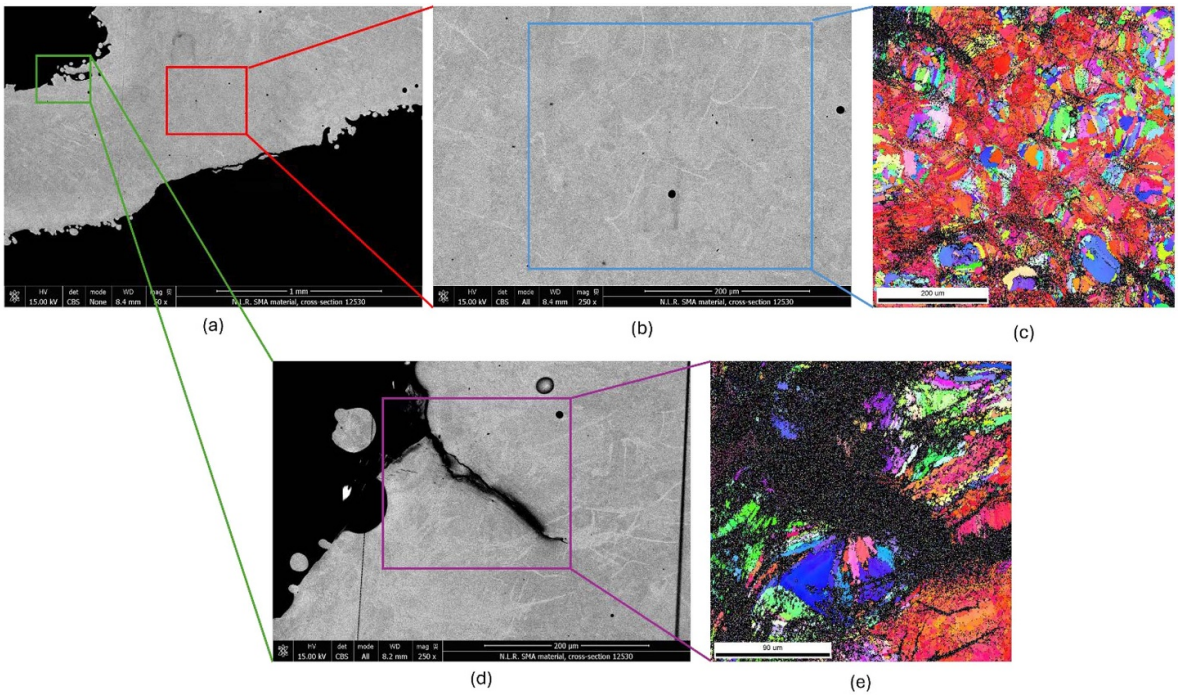

Figure 7. SEM-SE overview of the region near the fracture in Sample 4: (a) overview of the region, (b) magnification of the central part, with (c) its corresponding EBSD map; (d) magnification of a detected crack, with (e) its corresponding EBSD map.

4. Conclusion

This study investigated the fatigue behavior of LPBFed NiTi lattice structures across a broad range of cycles. By performing fatigue tests under varying load levels, an S–N curve following a power-law relationship was developed, revealing a consistent and predictable correlation between applied stress and fatigue life. This reliable fit enables confident extrapolation to different loading conditions, supporting the use of these lattices in cyclic applications.

The findings highlight how fatigue performance is governed not only by macroscopic stress-life trends but also by the complex interactions between phase transformations, lattice architecture, and manufacturing defects. Under higher loads, localized stresses can surpass the transformation threshold, triggering phase changes that affect energy dissipation and damage evolution within the material. The auxetic lattice design, with its negative Poisson's ratio, produces unconventional mechanical responses that cause uneven stress distribution and promote localized failures. Furthermore, manufacturing defects inherent to the LPBF process, especially at lattice corners and junctions, act as critical crack initiation sites, explaining instances of premature fatigue failure.

Together, these insights emphasize the importance of optimizing both design and manufacturing parameters to enhance the fatigue life of NiTi lattice structures for demanding cyclic applications.

Data availability statement

All data that support the findings of this study are included within the article (and any supplementary files).

Acknowledgments

The authors gratefully acknowledge the support of the Applied Research SIA Foundation through the KIEM HighTech program for the AM-SMART project (HT.KIEM.01.032). They also extend their sincere thanks to the mechanical testing laboratory at the Netherlands Aerospace Centre (NLR) in Marknesse, The Netherlands, for conducting the mechanical tests and providing SEM characterization. Special thanks are extended to Nicola Bennato from CNR-ICMATE for his valuable assistance in sample production.

Author contributions

Borit Zwerink 0009-0000-8170-6109
Formal analysis (equal), Investigation (equal), Writing – original draft (equal)

Carlo Alberto Biffi 0000-0001-5876-6007
Formal analysis (equal), Investigation (equal), Methodology (equal), Resources (equal), Writing – review & editing (equal)

Jacopo Fiocchi 0000-0002-7646-4595
Formal analysis (equal), Investigation (equal), Writing – review & editing (equal)

Mehrshad Mehrpouya 0000-0001-8939-7937
Conceptualization (equal), Formal analysis (equal), Funding acquisition (lead), Investigation (equal), Supervision (equal), Writing – review & editing (equal)

References

[1] Nespoli A, Grande A M, Passaretti F, Rigamonti D, Sala G and Bettini P 2023 Damping property of a NiTi auxetic structure fabricated through selective laser melting *Int. J. Adv. Manuf. Technol.* **126** 519–30

[2] Mehrpouya M and Elahinia M 2025 Introduction to additive manufacturing of shape memory materials *Additive Manufacturing of Shape Memory Materials* (Elsevier) pp 1–13

[3] Vanaei S, Mehrpouya M and Elahinia M 2025 L-PBF additive manufacturing of shape memory alloys *Additive Manufacturing of Shape Memory Materials* (Elsevier) *pp* 229–76

[4] Bregoli C, Fiocchi J, Biffi C A, Tuissi A, de Gallareta S L, Rodriguez-Florez N and Borghi A 2025 Biomechanical study of an additively manufactured NiTi patient-specific device for the treatment of craniosynostosis *J. Mech. Behav. Biomed. Mater.* **170** 107095

[5] Feng J, Fu J, Lin Z, Shang C and Li B 2018 A review of the design methods of complex topology structures for 3D printing *Vis. Comput. Ind. Biomed. Art* **1** 1–16

[6] Yang X, Yang Q, Shi Y, Yang L, Wu S, Yan C and Shi Y 2022 Effect of volume fraction and unit cell size on manufacturability and compressive behaviors of Ni-Ti triply periodic minimal surface lattices *Addit. Manuf.* **54** 102737

[7] Yan A, Cai W, Li H, Lu H, Lin J, Wang J, Zhang L C and Yang C 2024 Stable superelasticity with large recoverable strain in NiTi alloy via additive manufacturing *Mater. Sci. Eng.* **911** 146935

[8] Plocher J and Panesar A 2019 Review on design and structural optimisation in additive manufacturing: towards next-generation lightweight structures *Mater. Des.* **183** 108164

[9] Bici M, Brischetto S, Campana F, Ferro C G, Seclì C, Varetti S, Maggiore P and Mazza A 2018 Development of a multifunctional panel for aerospace use through SLM additive manufacturing *Proc. CIRP* **67** 215–20

[10] Bühring J, Nuño M and Schröder K-U 2021 Additive manufactured sandwich structures: mechanical characterization and usage potential in small aircraft *Aerosp. Sci. Technol.* **111** 106548

[11] Naghavi Zadeh M, Alijani F, Chen X, Dayyani I, Yasaee M, Mirzaali M J and Zadpoor A A 2021 Dynamic characterization of 3D printed mechanical metamaterials with tunable elastic properties *Appl. Phys. Lett.* **118** 211901

[12] Yang F *et al* 2017 Laser beam melting 3D printing of Ti6Al4V based porous structured dental implants: fabrication, biocompatibility analysis and photoelastic study *Sci. Rep.* **7** 45360

[13] Harris J, Winter R and McShane G J 2017 Impact response of additively manufactured metallic hybrid lattice materials *Int. J. Impact Eng.* **104** 177–91

[14] Yang E *et al* 2019 Effect of geometry on the mechanical properties of Ti-6Al-4V gyroid structures fabricated via SLM: a numerical study *Mater. Des.* **184** 108165

[15] Ataee A, Li Y, Fraser D, Song G and Wen C 2018 Anisotropic Ti-6Al-4V gyroid scaffolds manufactured by electron beam melting (EBM) for bone implant applications *Mater. Des.* **137** 345–54

[16] Yánez A, Herrera A, Martel O, Monopoli D and Afonso H 2016 Compressive behaviour of gyroid lattice structures for human cancellous bone implant applications *Mater. Sci. Eng. C* **68** 445–8

[17] Arabnejad Khanoki S and Pasini D 2013 The fatigue design of a bone preserving hip implant with functionally graded cellular material *J. Med. Devices* **7** 020907

[18] Mehrpouya M and Elahinia M 2025 *Additive Manufacturing of Shape Memory Materials: Techniques, Characterization, Modeling, and Applications* (Elsevier)

[19] Mehrpouya M, Alberto Biffi C, Lemke J N, Bregoli C, Fiocchi J, Mohajerani S, Tuissi A and Elahinia M 2024 Additive manufacturing of architected shape memory alloys: a review *Virtual Phys. Prototyp.* **19** e2414395

[20] Dadbakhsh S, Speirs M, Kruth J-P and Van Humbeeck J 2015 Influence of SLM on shape memory and compression behaviour of NiTi scaffolds *CIRP Ann.* **64** 209–12

[21] Biffi C A, Bassani P, Fiocchi J and Tuissi A 2020 Microstructural and mechanical response of NiTi lattice 3D structure produced by selective laser melting *Metals* **10** 814

[22] Zhang C, Jin J, He M and Yang L 2022 Compressive mechanics and hyperelasticity of Ni-Ti lattice structures fabricated by selective laser melting *Crystals* **12** 408

[23] Yu Z L, Chen L-X, Xin R I, Li J Y, Cao Q, Guo X and Qi Y C 2022 Mechanical analysis characteristics of bionic structure based on NiTi alloy additive manufacturing *Mater. Today Commun.* **33** 104313

[24] Dong G, Tang Y, Li D and Zhao Y F 2020 Design and optimization of solid lattice hybrid structures fabricated by additive manufacturing *Addit. Manuf.* **33** 101116

[25] Zhang Y, Attarilar S, Wang L, Lu W, Yang J and Fu Y 2021 A review on design and mechanical properties of additively manufactured NiTi implants for orthopedic applications *Int. J. Bioprinting* **7** 340

[26] Yuan B, Zhu M and Chung C Y 2018 Biomedical porous shape memory alloys for hard-tissue replacement materials *Materials* **11** 1716

[27] Saedi S, Saghaian S E, Jahadakbar A, Shayesteh Moghaddam N, Taheri Andani M, Saghaian S M, Lu Y C, Elahinia M and Karaca H E 2018 Shape memory response of porous NiTi shape memory alloys fabricated by selective laser melting *J. Mater. Sci., Mater. Med.* **29** 1–12

[28] Andani M T, Saedi S, Turabi A S, Karamooz M, Haberland C, Karaca H E and Elahinia M 2017 Mechanical and shape memory properties of porous $Ni_{50.1}Ti_{49.9}$ alloys manufactured by selective laser melting *J. Mech. Behav. Biomed. Mater.* **68** 224–31

[29] Chen W, Gu D, Yang J, Yang Q, Chen J and Shen X 2022 Compressive mechanical properties and shape memory effect of NiTi gradient lattice structures fabricated by laser powder bed fusion *Int. J. Extreme Manuf.* **4** 045002

[30] Jafarabadi A, Ferretto I, Mohri M, Leinenbach C and Ghafoori E 2023 4D printing of recoverable buckling-induced architected iron-based shape memory alloys *Mater. Des.* **233** 112216

[31] Robertson S, Pelton A and Ritchie R 2012 Mechanical fatigue and fracture of nitinol *Int. Mater. Rev.* **57** 1–37

[32] Kang G and Song D 2015 Review on structural fatigue of NiTi shape memory alloys: pure mechanical and thermo-mechanical ones *Theor. Appl. Mech. Lett.* **5** 245–54

[33] Maletta C, Sgambitterra E, Furgiuele F, Casati R and Tuissi A 2014 Fatigue properties of a pseudoelastic NiTi alloy: strain ratcheting and hysteresis under cyclic tensile loading *Int. J. Fatigue* **66** 78–85

[34] Schaffer J E 2009 Structure-property relationships in conventional and nanocrystalline NiTi intermetallic alloy wire *J. Mater. Eng. Perform.* **18** 582–7

[35] Niutta C B, Pagnoncelli A, Tridello A, Fiocchi J, Biffi C, Tuissi A and Paolino D S 2025 Very high cycle fatigue (VHCF) response of an additively manufactured nitinol *Int. J. Fatigue* **200** 109130

[36] Wei P, Hua P, Xia M, Yan K, Lin H, Yi S, Lu J, Ren F and Sun Q 2022 Bending fatigue life enhancement of NiTi alloy by pre-strain warm surface mechanical attrition treatment *Acta Mater.* **240** 118269

[37] Chen J, Yin H and Sun Q 2020 Effects of grain size on fatigue crack growth behaviors of nanocrystalline superelastic NiTi shape memory alloys *Acta Mater.* **195** 141–50
[38] Mahtabi M J, Shamsaei N and Mitchell M 2015 Fatigue of nitinol: the state-of-the-art and ongoing challenges *J. Mech. Behav. Biomed. Mater.* **50** 228–54
[39] Malito L G, Haghgouyan B, Bowers M L, Rosen A, Amin-Ahmadi B, Robertson S W and Ritchie R O 2024 Fatigue and fracture of small cracks in superelastic nitinol *Int. J. Fatigue* **183** 108208
[40] Launey M E, Ong I, Berg B T and Pelton A R 2023 Considerations on tension–tension fatigue predictions for nitinol *Shape Mem. Superelasticity* **9** 97–115
[41] Pelton A, Berg B, Saffari P, Stebner A and Bucsek A 2022 Pre-strain and mean strain effects on the fatigue behavior of superelastic nitinol medical devices *Shape Mem. Superelasticity* **8** 64–84
[42] Gugat J, Bechtold C, Chluba C, Quandt E and de Miranda R L 2020 High-cycle mechanical fatigue performance of sputtered nitinol *J. Mater. Eng. Perform.* **29** 1892–900
[43] Nezhad P S, Moore J A and Erdeniz D 2024 Effect of wire size on the functional and structural fatigue behavior of superelastic nitinol *Mater. Sci. Eng.* **895** 146218
[44] Alarcon E, Heller L, Chirani S A, Šittner P, Kopeček J, Saint-Sulpice L and Calloch S 2017 Fatigue performance of superelastic NiTi near stress-induced martensitic transformation *Int. J. Fatigue* **95** 76–89
[45] Tang D, Hu Y and Yang L 2023 New insights into the mechanical properties, functional fatigue, and structural fatigue of Ni-Ti alloy porous structures *Metals* **13** 931
[46] Bormann T, Friess S, de Wild M, Schumacher R, Schulz G and Müller B Determination of strain fields in porous shape memory alloys using micro-computed tomography *Developments in x-ray tomography VII: SPIE* pp 424–32
[47] Jahadakbar A, Nematollahi M, Safaei K, Bayati P, Giri G, Dabbaghi H, Dean D and Elahinia M 2020 Design, modeling, additive manufacturing, and polishing of stiffness-modulated porous nitinol bone fixation plates followed by thermomechanical and composition analysis *Metals* **10** 151
[48] Gu D, Ma C, Dai D, Yang J, Lin K, Zhang H and Zhang H 2021 Additively manufacturing-enabled hierarchical NiTi-based shape memory alloys with high strength and toughness *Virtual Phys. Prototyp.* **16** S19–S38
[49] Saint-Sulpice L, Legrand V, Arbab-Chirani S, Calloch S and Doudard C 2022 Fatigue life study of superelastic NiTi shape memory alloys using self-heating under cyclic loading method *Int. J. Fatigue* **165** 107208
[50] Koschella K, Degel C and Hempel P 2023 Numerical investigation on the effect of inclusions on the local fatigue strain in superelastic NiTi alloy *Shape Mem. Superelasticity* **9** 74–86
[51] Biffi C, Soyarslan C, Fiocchi J, Bregoli C, du Plessis A, Tuissi A and Mehrpouya M 2024 Additive manufacturing of NiTi architected metamaterials *Addit. Manuf. Lett.* **10** 100216
[52] Biffi C A, Soyarslan C, Fiocchi J, Bregoli C, Tuissi A and Mehrpouya M 2023 Functional performance of NiTi shape memory architected structures produced by laser powder bed fusion (LPBF) *Trans. Addit. Manuf. Meets Med.* **5** 821
[53] Speirs M, Van Hooreweder B, Van Humbeeck J and Kruth J-P 2017 Fatigue behaviour of NiTi shape memory alloy scaffolds produced by SLM, a unit cell design comparison *J. Mech. Behav. Biomed. Mater.* **70** 53–59
[54] Ren Y, Li Y, Yang L, Chen Y, Yan C, Liu B, Cai X, Zhang M and Shi Y 2024 Compressive properties and fatigue performance of NiTi lattice structures optimized by TPMS *Mater. Sci. Addit. Manuf.* **3** 3380
[55] Moutablaleh H, Abdelhady E S, Vaneker T, Gibson I and Mehrpouya M 2025 A comparative analysis of functional performance in additively manufactured NiTi, Ti-6Al-4V, and 316L stainless steel architected metastructures *J. Mech. Behav. Biomed. Mater.* **169** 107071